INTERNATIONAL JOURNAL FOR NUMERICAL METHODS IN FLUIDS
Int. J. Numer. Meth. Fluids 2002; **40**:497–505 (DOI: 10.1002/fld.314)

A study of flow arising from insect wing flapping motion

J. Szmelter* and R. Żbikowski

RMCS Cranfield University, Shrivenham, Swindon, SN6 8LA, U.K.

SUMMARY

We have modelled the aerodynamics of the flapping insect wing to provide insight into the aerodynamics of flapping wing micro air vehicles. The complexities of the physics of the flow have been highlighted and methodologies which could be used to explore it have been defined. Initial solutions have been obtained which qualitatively agree with experiments. Copyright © 2002 John Wiley & Sons, Ltd.

KEY WORDS: aerodynamics; bioaerodynamics; insect wing; micro air vehicles

1. INTRODUCTION

The main objective of this work is to provide more insight into the little-known and complex [1, 2] bioaerodynamics of insect flight, with a view of using the insight for the design of flapping wing micro air vehicles [3].

A methodology for modelling of the aerodynamics of the flapping insect wing is proposed in this paper. Numerical simulations will be applied to study the novel design concepts of flapping wing micro air vehicles (MAVs) [3]. The development of small (ca. six inches, or hand-held) autonomous flying vehicles is motivated by a need for intelligent reconnaissance robots, capable of discreetly penetrating confined spaces and manoeuvring in them without the assistance of a human telepilot [4]. The reported work is part of a larger multidisciplinary project involving materials, sensors, actuators, navigation, guidance and control, and biological experiments [5].

A previous numerical study of note on insect flight is the paper by Liu and Kawachi [2] which focused on numerical reproduction of the flow generated by a tethered hawkmoth *Manduca sexta* [6]. In this paper we consider the wing of a *Bibio* fly [7, p. 46], whose semi-span has been scaled up to 126 millimetres. The assumed kinematics is similar to that observed for the hawkmoth. Numerically, we use the artificial compressibility assumption, as in Reference [2], but apply a solver and meshing which are different from those used by Liu and Kawachi. In particular, the hybrid meshes employed are well suited for capturing viscous effects and allow handling of complicated wing shapes. This approach is better suited to the design of flapping wings for MAVs, where frequent changes of the wing geometric and kinematic parameters may be required and, in the future, inclusion of the vehicle's body.

*Correspondence to: J. Szmelter, RMCS Cranfield University, DEOS, Shrivenham, Swindon SN6 8LA, U.K.

Contract/grant sponsor: EPSRC; contract/grant number: GR/M78472

Received May 2001
Revised September 2001

2. KINEMATICS OF INSECT-LIKE FLAPPING

Insects fly by oscillating (frequency range: 5–200 Hz) and rotating their wings through large angles, while sweeping them forwards and backwards. This mode of flying relies on unsteady aerodynamics, producing high lift coefficients (peak C_L of 3 is typical) and excellent manoeuvrability. The unsteady mechanism varies with different insects: the most important mechanism is a bound, leading-edge vortex [6].

Recall that the basic formula for the wing aerodynamic lift force is $L = 0.5\rho SV^2 C_L$, where ρ is the air density, S is the wing area and V the relative (accounting for wind effects) velocity of the wing with respect to air. The value of the (dimensionless) lift coefficient C_L depends mainly on the wing design and angle of attack and seldom exceeds 1.2 for conventional aeronautical applications. For unsteady aerodynamics, the lift force will be time-varying $L = L(t)$ and this is reflected by time-variance of the lift coefficient $C_L = C_L(t)$. Hence, its peak values of 3 during the insect wingbeat cycle are remarkable when compared with conventional flying machines. The main consequence for insect flight is generation of high lift at low speeds thus enabling slow, but highly manoeuvrable and power efficient flight (for insects speeds of a few mph are typical).

The wingbeat cycle can be divided into two phases: downstroke and upstroke (see Figures 1 and 2). At the beginning of downstroke, the wing (as seen from the front of the insect) is in the uppermost and rearmost position with the leading edge pointing forward. The wing is then pushed downwards and forwards and rotated continuously, so that the angle of attack changes considerably during this downward motion. At the end of the downstroke, the wing is twisted rapidly, so that the leading edge points backwards, and the upstroke begins. During the upstroke the wing is pushed upwards and backwards and rotated again, which changes the angle of attack throughout this motion. At the highest point, the wing is twisted again, so that the leading edge points forward and the next downstroke begins.

Insect wing flapping occurs in a stroke plane that generally remains at the same orientation to the body and is either horizontal or inclined, see Figure 2. In forward flight the downstroke lasts longer than the upstroke, because of the need to generate thrust. In hover they are equal, resulting in the wing tip tracing a flat figure of eight (as seen from the insect's side).

Insect wing flapping is a special combination of three motions: (i) oscillation, or the up and down motion (the angle θ in Figure 3), (ii) rotation, or pitching and plunging (the angle α in Figure 3), and (iii) sweep, or forwards and backwards motion (the angle ϕ in Figure 3). Note that in Figure 3 the sense of the angles is indicated by the arrow of the corresponding arc. Thus, θ is positive when the wing moves upwards (from the y-axis towards the z-axis), α is positive when the wing pitches (the leading edge is above the insect) and ϕ is positive when the wing moves backwards (from the y-axis towards the x-axis).

The kinematic data used in this paper have been kindly provided by Ellington (based on References [8–10]) and are very similar to those used in Reference [2]. Each component motion, i.e. in θ, α and ϕ, is periodic and therefore can be represented by Fourier series. Based on an experimental sensitivity study Ellington has found that it suffices to truncate the series at the third harmonic:

$$x_i(t) = \frac{1}{2}a_0^i + \sum_{k=1}^{3}(a_k^i \cos k\omega_0 t + b_k^i \sin k\omega_0 t), \quad i = 1,2,3 \tag{1}$$

where $x := [\theta\ \alpha\ \phi]^T$.

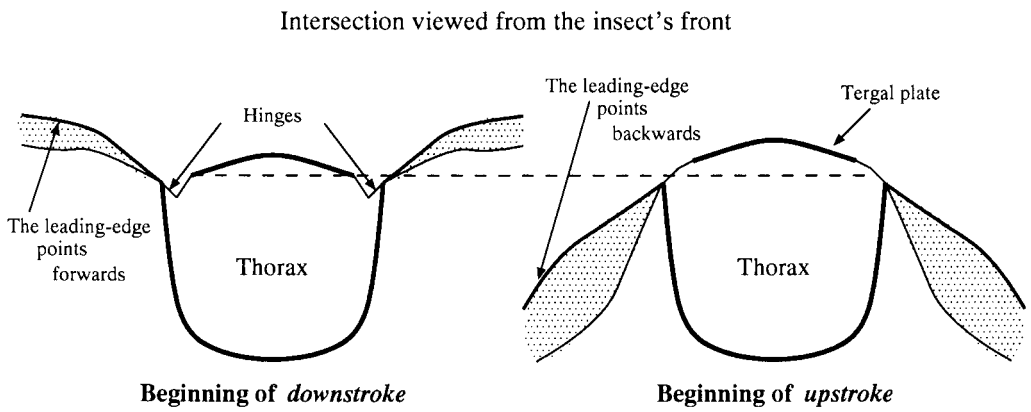

Figure 1. Insect wing flapping is a periodic motion and each cycle is composed of the downstroke and upstroke. At the end of each half-cycle the wing reverses its direction.

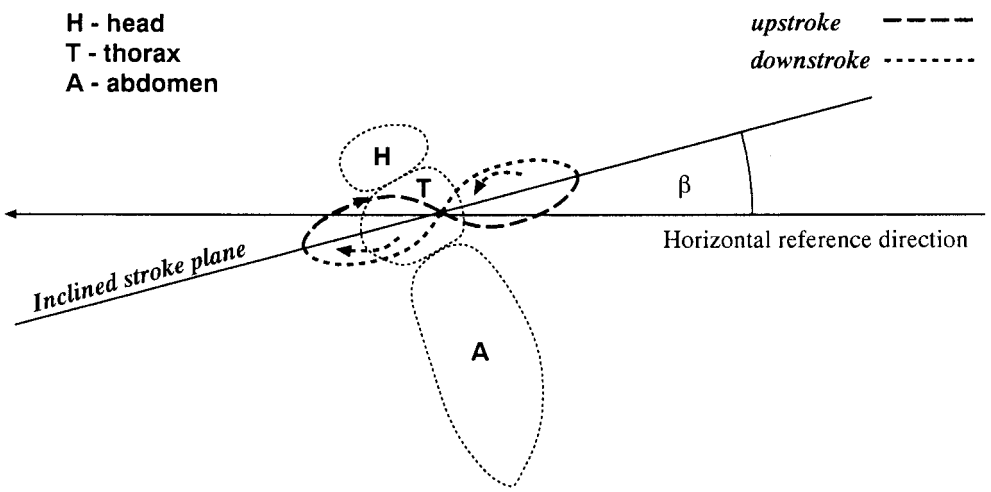

Figure 2. Typical motions of insect wing in hover. Insect body is orientated horizontally, while the wing tip traces a flat figure of eight around the stroke plane. The stroke plane is inclined by the angle β.

The oscillation causes the wing to move above and below the stroke plane and its amplitude is not usually high; in our case $\theta \in [-11.35°, 6.15°]$. The changes in wing incidence are more visible: $\alpha \in [51.83°, 138.40°]$. Wing sweep is also pronounced with $\phi \in [-46.50°, 64.26°]$, where the negative values mean that the wing is the forward part of the figure of eight. Finally, the stroke plane is inclined at $\beta = 15°$. Since α varies around $\alpha_c := (\alpha_{\max} + \alpha_{\min})/2 = 95.12°$ by $A := \alpha_{\max} - \alpha_c = 43.29°$, the effective incidence can be modelled as an oscillation around $\beta + \alpha_c$ with amplitude A. A similar approach is applicable to ϕ and θ.

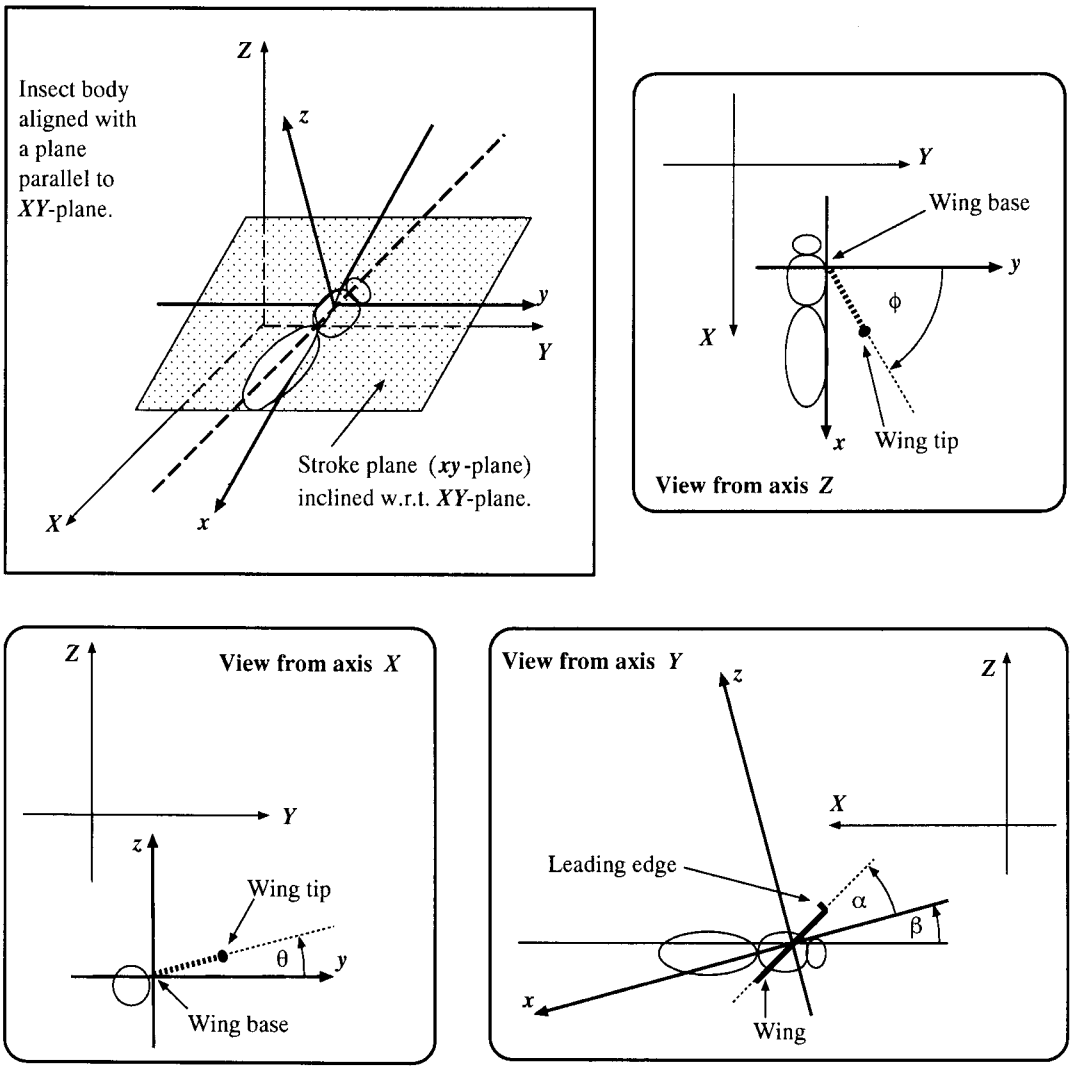

Figure 3. The co-ordinate system, adopted by Willmott and Ellington [8–10] for their study of flight in the hawkmoth *Manduca sexta*, and used in this paper. The origin of the right-hand *xyz* system is at the wing base (where the wing is attached to the body). The *xy*-plane coincides with the stroke plane and the *z*-axis is orthogonal to this plane. The stroke plane is inclined with respect to the *XY*-plane of the external *XYZ* reference frame; in this frame the insect body is orientated horizontally. In hover the wing moves above and below the stroke plane, and forwards and backwards along the plane. Coupled with the wing rotation, this makes the wing tip trace a flat figure of eight with the stroke plane providing the symmetry axis; see also Figure 2.

3. CFD METHODOLOGY

3.1. Flow solution and dynamic remeshing

Speed characteristics of this problem are low or zero, therefore the flow is treated as an incompressible fluid. At low Reynolds numbers (up to 9×10^3), which are typical for insect flight, the flow can be assumed to be dominantly laminar. Such flow can be described by the following differential form of the Navier–Stokes equations written in the Eulerian co-ordinate system:

$$\frac{\partial \mathbf{w}}{\partial t^*} + \mathbf{\Phi}\left(\frac{\partial \mathbf{f}}{\partial x} + \frac{\partial \mathbf{g}}{\partial y} + \frac{\partial \mathbf{h}}{\partial z}\right) = 0 \tag{2}$$

where the vector of dependent variables $\mathbf{w}$ and the flux vectors $\mathbf{f}, \mathbf{g}, \mathbf{h}$ are given by:

$$\begin{aligned} \mathbf{w} &= [p \quad u \quad v \quad w]^{\mathrm{T}} \\ \mathbf{f} &= [u \quad u^2 + p - \tau_{xx} \quad uv - \tau_{xy} \quad uw - \tau_{xz}]^{\mathrm{T}} \\ \mathbf{g} &= [v \quad vu - \tau_{yx} \quad v^2 + p - \tau_{yy} \quad vw - \tau_{yz}]^{\mathrm{T}} \\ \mathbf{h} &= [w \quad wu - \tau_{zx} \quad wv - \tau_{zy} \quad w^2 + p - \tau_{zz}]^{\mathrm{T}} \end{aligned} \tag{3}$$

and matrix $\mathbf{\Phi}$ can be written as

$$\mathbf{\Phi} = \begin{bmatrix} c^{*2} & 0 & 0 & 0 \\ 0 & 1 & 0 & 0 \\ 0 & 0 & 1 & 0 \\ 0 & 0 & 0 & 1 \end{bmatrix} \tag{4}$$

where p indicates pressure, u, v, w are the Cartesian velocity components in x, y, z directions and τ_{ij} are the components of the shear stress tensor. This system of equations is closed by the ideal gas state equation.

It can be noticed that the continuity equation, representing the incompressibility condition, is modified by adding the artificial compressibility term:

$$\frac{\partial p}{\partial t^*} \frac{1}{c^{*2}} \tag{5}$$

where c^* corresponds to a finite artificial speed of sound and t^* indicates pseudo time. (For incompressible flows the speed of sound is infinite.) In this way, the mathematical character of Equations (2) is changed to a system of hyperbolic equations for which an explicit flow solver can be employed. As in Reference [11], c^* is chosen to achieve a compromise between maximum and minimum wave speeds and to maintain both accuracy and stability. Thus, $(c^*)^2 = C(u^2 + v^2 + w^2)$, where the constant C is of the order of unity.

The numerical solution is based on the three dimensional. Runge–Kutta, explicit, code. To avoid numerical stability limitations imposed for the explicit solvers on the time step by the CFL conditions for incompressible flows, the above artificial compressibility approach has been employed. The method, originally proposed by Chorin [12], has already been used in the context of flapping wing modelling by Liu and Kawachi [2]. In the work presented here, the developments reported in Reference [11] have been closely followed.

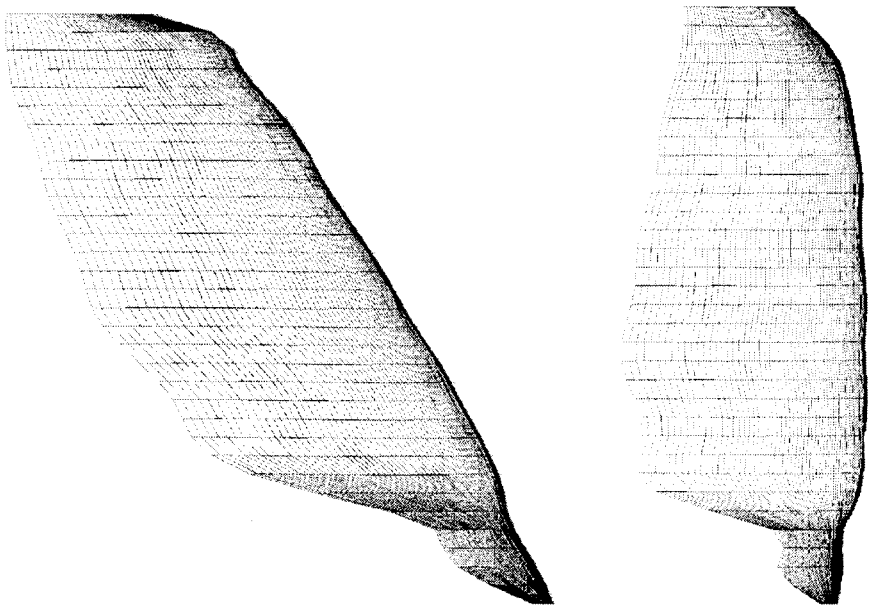

Figure 4. The effect of sweep angle on the surface mesh: (a) at $0.5T$ for $\phi = -45.77°$, $\theta = 2.21°$ and $\alpha = 92.69°$; (b) at $0.25T$ for $\phi = 3.47°$, $\theta = -4.73°$ and $\alpha = 63.92°$.

In steady state, time derivatives reduce to zero, and solutions of the systems of modified equations and the original incompressible flow Navier–Stokes equations become equivalent. The artificial compressibility method has been further extended (as shown for example in Reference [2]) to treat time-dependent flows. This extended, dual time-stepping method relies on introduction of time intervals. Within each interval, additional iterations in pseudo time are performed and the assumption is made that the flow recovers physical time derivative in the limit.

The spatial discretization is based on the three-dimensional Runge–Kutta, finite-volume code. This dual-mesh, edge-based, finite-volume code is valid for general hybrid meshes, although in this application only hexahedral cells are used. Artificial dissipation of Jameson is used [13].

Dynamic remeshing produces errors due to the moving mesh. In order to ensure that the mesh changes do not affect the flow field, the geometric conservation equations are additionally solved during time integration [14]. These are: (i) volume conservation law, obtained by applying the continuity equation to a flowfield with zero velocity and constant density, (ii) surface conservation law, obtained by applying the continuity equation to a constant-density flow in arbitrary direction on a fixed grid. For this solution the same integration scheme is used as for the conservation law of the fluid.

In the presented calculation the structured single block C-H $192 \times 64 \times 32$ mesh is used and is generated by the fast conformal mapping technique. The movement of the wing is

prescribed as explained in the previous section. At present the mesh is regenerated at every time step. Sample surface mesh plots at the most characteristic data points (corresponding to $0.25T, 0.5T$ times in the flapping cycle) are shown in Figure 4.

3.2. Numerical results

Sample calculations illustrating current capabilities of the method and providing a preliminary insight into the aerodynamic behaviour of flapping wing have been performed. At this stage the choice of the wing planform and shape of aerofoils forming the wing are still open questions. In the presented calculations the choice of the planform has been inspired by the geometry of the wing of a *Bibio* fly. The wing semi-span is 126 mm, the Mach number is zero and the Reynolds number 5×10^3.

A constant aerofoil section was used along the wing span and scaled with respect to local chord to fit the planform. A symmetric NACA0012 aerofoil with thickness decreased 0.1 times was chosen.

The values of C_L obtained were within the range -1.0 and 2.8 and a typical time history after the flow has been established is shown for two cycles in Figure 6. A leading edge recirculation was detected, qualitatively consistent with experimental findings [6], but is difficult

Figure 5. 3-D vectors indicating the presence of a leading-edge vortex.

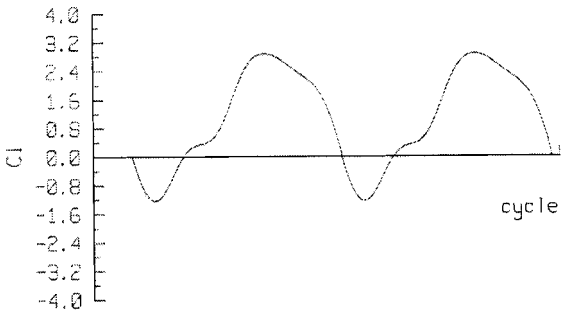

Figure 6. The lift coefficient for two cycles, after convergence to established cyclical flow.

to visualize, as seen in Figure 5. However, a clear presence of recirculation was seen from examining directions and values of velocity components at relevant grid positions. We intend to improve data analysis routines for this purpose.

The compressible flow option of the code and wing movement were validated for a very long wing built on an oscillating NACA0012 aerofoil. The validation of the incompressible flow option was conducted for a flow around a cylinder.

4. CONCLUSIONS

This paper reports the current status of a project investigating aerodynamic aspects of flapping MAVs. The complexities of the physics of the flow have been highlighted and methodologies which could be used to explore it have been defined. Initial solutions have been obtained which qualitatively agree with experiments. The next step will be to perform quantitative validation with forthcoming new data from both biological and engineering experiments.

ACKNOWLEDGEMENTS

This work has been supported by the EPSRC Grant GR/M78472 'Flapping Flight Aerodynamics of Autonomous Micro Air Vehicles'.

REFERENCES

1. Ellington CP. Unsteady aerodynamics insect flight. In *Biological Fluid Dynamics*, Ellington CP, Pedley TJ (eds.), vol. 49, *Symposia of the Society for Experimental Biology*, 1995; 109–129.
2. Liu H, Kawachi K. A numerical study of insect flight. *Journal of Computational Physics* 1998; **146**(1): 124–156.
3. Żbikowski R. Flapping wing autonomous micro air vehicles: Research programme outline. In *Fourteenth International Conference on Unmanned Air Vehicle Systems*, vol. [Supplementary Papers], 1999; 38.1–38.5.
4. Żbikowski R. Flapping wing micro air vehicle: A guided platform for microsensors. In *Royal Aeronautical Society Conference on Nanotechnology and Microengineering for Future Guided Weapons*, 1999; 1.1–1.11.
5. Żbikowski R, Pedersen CB, Hameed A, Friend CM, Barton PC. Current research on flapping wing micro air vehicles at Shrivenham. In *AVT Symposium on Unmanned Vehicles for Aerial, Ground and Naval Military Operations*, *Ankara*, *Turkey*, 2000; 16.1–16.14.
6. Ellington CP, van den Berg C, Willmott AP, Thomas ALR. Leading-edge vortices in insect flight. *Nature* 1996; **384**(6610):626–630.

7. Gullan PJ, Cranston PS. *The Insects*: *An Outline of Entomology*. Chapman & Hall: London, 1994.
8. Willmott AP, Ellington CP. Measuring the angle of attack of beating insect wings: Robust three-dimensional reconstruction from two-dimensional images. *Journal of Experimental Biology* 1997; **200**(21):2693–2704.
9. Willmott AP, Ellington CP. The mechanics of flight in the hawkmoth *Manduca sexta*. I. Kinematics of hovering and forward flight. *Journal of Experimental Biology* 1997; **200**(21):2705–2722.
10. Willmott AP, Ellington CP. The mechanics of flight in the hawkmoth *Manduca sexta*. II. Aerodynamic consequences of kinematic and morphological variation. *Journal of Experimental Biology* 1997; **200**(21): 2723–2745.
11. Farmer J, Martinelli L, Jameson A. Fast multigrid method for solving incompressible hydrodynamic problems with free surfaces. *AIAA Journal* 1994; **32**(6):1175–1182.
12. Chorin A. A numerical method for solving incompressible viscous flow problems. *Journal of Computational Physics* 1967; **2**:12–26.
13. Jameson A. Analysis and design of numerical schemes for gas dynamics. 2. Artificial diffusion and discrete shock structure. *International Journal of Computational Fluid Dynamics* 1995; **5**(1–2):1–38.
14. Zhang H, Reggio M, Trepanier JY, Camarero R. Discrete form of the GCL for the moving meshes and its implementation in CFD schemes. *Computers & Fluids* 1993; **22**(1):9–23.

